J. Phase Equilib. Diffus. (2021) 42:864–878
https://doi.org/10.1007/s11669-021-00928-3

Thermodynamic Assessment of the Ternary B-Hf-Zr System with Refined B-Hf Description

Yafei Pan[1,2] · Lei Huang[1,2] · Jiuxing Zhang[1,2] · Yong Du[3] · Fenghua Luo[3] · Shuyan Zhang[4]

Submitted: 6 July 2021 / in revised form: 9 September 2021 / Accepted: 10 September 2021 / Published online: 8 November 2021

Abstract Thermodynamic assessment of the ternary system B-Hf-Zr has been conducted by modeling the Gibbs energy of all individual phases using the CALPHAD (CALculation of PHAse Diagrams) approach. There is no ternary compound in this system. The individual solution phases, i.e., liquid, (βHf,βZr), HfB and $(Hf,Zr)B_2$ have been modeled. The modeling covers the whole composition and temperature ranges. The Gibbs energies of HfB_2 and HfB in the B-Hf system were reassessed using the two-sublattice models $(B,Hf)_1(B,Hf)_2$ and $(Hf)_1(B,Hf)_1$, respectively. A set of self-consistent thermodynamic parameters for the B-Hf-Zr system was obtained by considering the phase diagram data in the ternary system. Comprehensive comparisons between the calculated and measured phase diagram and thermodynamic data show that the experimental information was satisfactorily accounted for by the present thermodynamic description. The liquidus projection and reaction scheme of the B-Hf-Zr system are also presented.

✉ Yafei Pan
pan2018@hfut.edu.cn

1 School of Materials Science and Engineering, Hefei University of Technology, Hefei 230009, Anhui, People's Republic of China

2 Engineering Research Center of High-Performance Copper Alloy Materials and Processing, Ministry of Education, Hefei University of Technology, Hefei 230009, Anhui, People's Republic of China

3 State Key Laboratory of Powder Metallurgy, Central South University, Changsha 410083, Hunan, People's Republic of China

4 Centre of Excellence for Advanced Materials, Songshan Lake, Dongguan 523808, Guangdong, People's Republic of China

Keywords B-Hf-Zr · borides · phase diagram · thermodynamics

1 Introduction

Refractory diborides of zirconium and hafnium based ceramics are currently considered materials of great interest for ultrahigh-temperature applications because of their combination of engineering properties, such as high melting point (3245 and 3380 °C, respectively), high hardness (> 20 GPa), superior thermal shock and oxidation resistance.[1–3] Despite possessing excellent set of properties, their low self-diffusion coefficient and covalent bonding restrict achieving full densification at temperatures below 2000 °C.[4] Recently, HfB_2 and ZrB_2 composites prepared via in situ reactive sintering were reported to have high density, fine microstructures and excellent mechanical properties.[5] In the process of designing the reaction routes to fabricate diboride ceramics, a large degree of mechanical testing is expensive and time-consuming, while computational thermodynamics on the basis of phase equilibria and thermodynamic properties has shown to be a powerful tool.[6]

The CALPHAD (CALculation of PHAse Diagrams) approach is a useful tool to establish thermodynamic databases, which are the bases for the prediction of thermodynamic properties, phase diagrams, diffusion[7] and phase-field simulations.[8] In order to obtain the thermodynamic data of HfB_2 or ZrB_2, and further develop the thermodynamic databases of multicomponent refractory metal borides, knowledge concerning phase equilibria and thermodynamic properties of the B-Hf-Zr ternary system is of fundamental importance. The present work is thus

intended to (I) critically evaluate the experimental phase diagram information and thermodynamic data in the B-Hf-Zr ternary system and its constituent binary systems from the literature, (II) provide an improved thermodynamic description of the constituent binary B-Hf system system, and (III) develop self-consistent thermodynamic description for the ternary B-Hf-Zr system.

2 Evaluation of Phase Diagram Data in the Literature

In the present assessment, the published phase diagram, and thermodynamic data of B-Hf-Zr system are critically reviewed. To facilitate reading, the symbols to denote the stable phases in the B-Hf-Zr system are summarized in Table 1.

2.1 Binary Systems

The thermodynamic modeling of the B-Hf binary system were firstly performed by Rogl and Potter[9] to describe the phase relationships investigated by Rudy and Windisch.[10] Then, Bittermann and Rogl[11] reassessed the binary B-Hf system, incorporating the available experimental high-temperature heat content and specific heat data into the description of hafnium diboride, and the boron solubility in the unary metal phases was presented. In their assessments, the HfB_2 and HfB phases were treated as stoichiometric compounds $(Hf)_1(B)_2$ and $(Hf)_1(B)_1$. Since HfB_2 and ZrB_2 have the same AlB_2-type structure and form a continuous solution $(Hf,Zr)B_2$ in the B-Hf-Zr ternary system, the same kind of sublattice model needs to be used in the present modification of the B-Hf system. The model $(B,Me)_1(B,Me)_2$ (Me=Hf or Zr), which was successfully applied to describe the solubility of ZrB_2 (66.7 to 66.9 at.%) in the B-Zr system,[6] has been employed to describe the Gibbs energy of HfB_2. In addition, the thermodynamic model of the HfB phase was also adjusted as $(Hf)_1(B,Hf)_1$, which is accord with model for the TiB phase in the B-Ti system.[12] The thermodynamic parameters for the other phases including L, (αHf), (βHf) and (βB) in the B-Hf system were the same as those selected by Bittermann and Rogl.[11] The heat capacity,[11,14-17] formation enthalpy[11,13,18-27] and entropy[11,13,17] of HfB_2 and HfB are also considered in the present optimization.

The B-Zr system is composed of liquid, (αZr), (βZr), (βB), ZrB, ZrB_2, and ZrB_{12}. It is worth noting that there exists a dispute regarding the stability of the ZrB phase. Glaser and Post[28] found that the ZrB phase of face-centered cubic structure has an extremely narrow range of stability and very rapid quenching is necessary to retain it at room temperature. The recommended temperature range for stabilizing the ZrB phase was from 1523 to 1073 K.[28] Although Rudy and Windisch[29] and Portnoi et al.[30,31] did not observe this phase in their studies, its existence was confirmed later by Nowotny, Shulishova and Haggerty,[32-34] respectively. Champion and Hagege[35–37] further confirmed the existence of ZrB with a peritectoid reaction by X-ray diffraction (XRD) and transmission electron microscopy (TEM) analysis, and even found that this phase was easily stabilized to room temperature. Moreover, this phase was identified with the NaCl type structure (space group *Fm*-3*m*, No. 225) by selected-area electron and X-ray diffraction, and the lattice parameter of which, measured by X-ray experiments, is about 4.71 Å. Despite several investigations[34,37] have concluded NaCl-type ZrB to be an impurity stabilized phase, the discussion given above has led us to accept NaCl-Type ZrB as a stable binary

Table 1 Crystallographic information and thermodynamic models to describe the phases in the B-Hf-Zr system.

Phase	Pearson symbol	Space group	Model	Phase description
Liquid	…	…	$(B,Hf,Zr)_1$	Liquid solution
(βHf,βZr)	*cI*2	*Im*-3*m*	$(Hf,Zr)_1(B,Va)_3$	Solid solution based on bcc (βHf) or (βZr)
(αHf,αZr)	*hR*2	$P6_3/mmc$	$(Hf,Zr)_1(B,Va)_{0.5}$	Solid solution based on hcp (αHf) or (αZr)
$(Hf,Zr)B_2$	*hP*3	*P6/mmm*	$(B,Hf,Zr)_1(B,Hf,Zr)_2$	Solid solution based on HfB_2 or ZrB_2
HfB	*oP*8	*Pnma*	$(Hf,Zr)_1(B,Hf)_1$	Solid solution based on HfB
ZrB	*cF*8	*Fm*-3*m*	$(Zr)_1(B)_1$	Stoichiometric compound of ZrB
ZrB_{12}	*cF*52	*Fm*-3*m*	$(Hf,Zr)_1(B)_{12}$	Solid solution based on ZrB_{12}
(βB)	*hR*105	*R*-3*m*	$B_{93}(B,Zr)_{12}$	Solid solution based on rhombohedral B

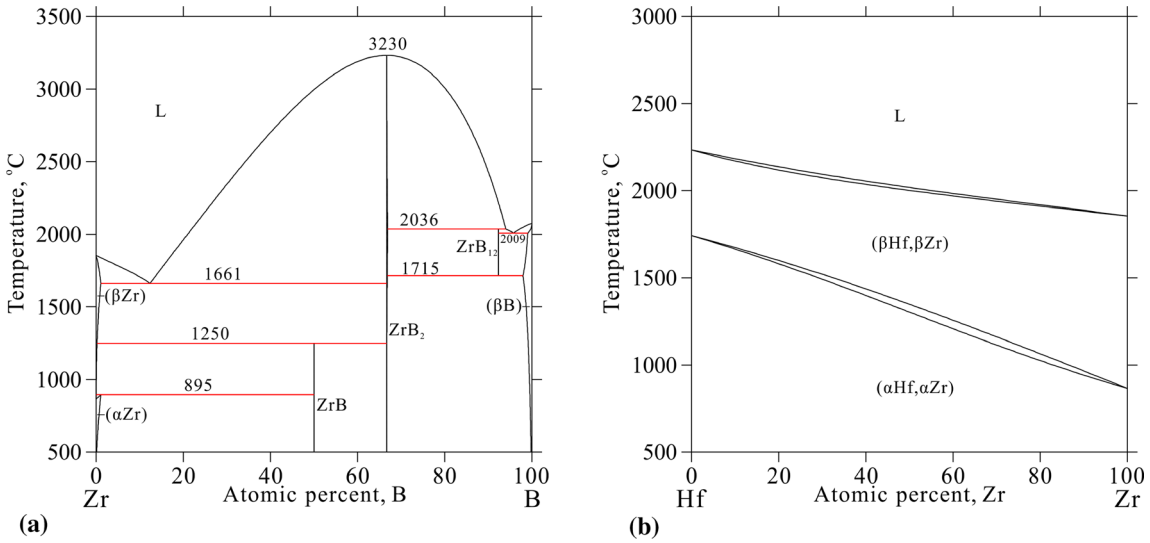

Fig. 1. Calculated binary phase diagrams: (a) B-Zr system[6] and (b) Hf-Zr system[38]

phase. The thermodynamic parameters of B-Zr assessed by Pan et al.[6] were reliable and adopted in this modeling.

The Hf–Zr system presents the phases liquid, (βHf,βZr) and (αHf,αZr). There is no intermediate compound in this binary system. In the present optimization, the thermodynamic parameters of the Hf–Zr system are directly taken from the work of Bittermann and Rogl.[38] The calculated B-Hf and Hf-Zr phase diagrams are shown in Fig. 1(a) and (b), respectively.

2.2 Ternary Systems

By means of optical microscopy (OM), X-ray diffraction (XRD), and the melting point techniques, Harmon[39] and Rudy[40] carried out the extensive work to investigate the B-Ti-Zr ternary phase diagram. The phase relationships included several vertical sections ($Hf_{70}B_{30}$-$Zr_{70}B_{30}$ and $Hf_{50}B_{50}$-$Zr_{50}B_{50}$), isothermal sections (varied from 1200 to 3300 °C), three-dimensional isometric view of the ternary system, and reaction scheme. However, the experimental details or original experimental data were not presented in the published vertical and isothermal sections. According to the study from Ref 39 and 40, no ternary compound was detected in the temperature range from 1200 °C up to the melting temperatures of alloys. For the isothermal section at 1200 °C, the lattice parameters of the samples with compositions of 66.67 at.% B were found to follow the Vegrad's law, which demonstrated that a continuous solid solution was formed between HfB_2 and ZrB_2. The solid solution $(Hf,Zr)B_2$ is stable until 3230 °C, at which the ZrB_2 phase melts congruently.

According to Harmon[39] and Rudy,[40] one solid invariant reaction, i.e., (βHf,βZr)+HfB=$(Hf,Zr)B_2$+(αHf) occurred at 1240 °C. The primary crystallization phases, namely those of HfB, $(Hf,Zr)B_2$, (βHf,βZr) and (βB) can be observed in the liquidus projection of the B-Hf-Zr system. The two following invariant transition equilibria were confirmed by Ref 39 and 40: L+$(Hf,Zr)B_2$=(βB)+ZrB_{12} at 2020 °C and L+HfB=$(Hf,Zr)B_2$+(-βHf,βZr) at 1715 °C with the liquid composition of 13.35 at.% B and 20.05 at.% Hf. They also reported the variations of temperature and B content of the quasi-binary liquid reactions: L=$(Hf,Zr)B_2$+(βHf,βZr) and L=HfB+(βHf,βZr). By means of Pirani-Alterthum method applied to 8 alloys, the melting temperatures of the $(Hf,Zr)B_2$ solid solution was constructed by Harmon[39] and Rudy.[40] The data mentioned above are all considered in the present optimization.

To establish thermodynamic database for the B-Hf-Ni-Ti-Zr system, Cacciamani et al.[41] assessed the B-Hf-Zr system. In their study, the isothermal section at 1500 and 1775 °C, and liquidus projection were considered. The phase equilibria in the temperature range from 1775 °C up to the melting temperatures were not included in their

optimization. The calculated[41] and measured[39,40] temperatures for the invariant reactions L+HfB=(Hf,Zr)B_2+(βHf, βZr) differ up to 48 °C.

To better reproduce the experimental information,[10,11,13–27,39,40] the HfB_2 and HfB phases of the binary B-Hf system and the whole ternary B-Hf-Zr system were modeled in detail in the present work.

3 Thermodynamic Models

In the present modeling, the Gibbs energy functions for the elements B, Hf and Zr are taken from the SGTE compilation by Dinsdale.[42] The thermodynamic parameters in the B-Zr, Hf-Zr and B-Hf binary constituent systems are taken from Pan et al.,[6] Bittermann and Rogl[38] and Bittermann and Rogl[11] with the HfB_2 and HfB phases modified in the present work. Different thermodynamic models were applied depending on the crystal structure and thermodynamic property of each phase.

3.1 Liquid

The liquid phase is described as substitutional solution, and the Gibbs energy is expressed by the Redlich-Kister-Muggianu polynomial:[43,44]

$$\begin{aligned} {}^{0}G_m^L = {} & x_{\mathrm{B}} \cdot {}^{0}G_{\mathrm{B}}^L + x_{\mathrm{Hf}} \cdot {}^{0}G_{\mathrm{Hf}}^L + x_{\mathrm{Zr}} \cdot {}^{0}G_{\mathrm{Zr}}^L \\ & + RT \cdot (x_{\mathrm{B}} \cdot \ln x_{\mathrm{B}} + x_{\mathrm{Hf}} \cdot \ln x_{\mathrm{Hf}} + x_{\mathrm{Zr}} \cdot \ln x_{\mathrm{Zr}}) \\ & + x_{\mathrm{B}} \cdot x_{\mathrm{Hf}} \cdot L_{\mathrm{B,Hf}}^L + x_{\mathrm{B}} \cdot x_{\mathrm{Zr}} \cdot L_{\mathrm{B,Zr}}^L + x_{\mathrm{Hf}} \cdot x_{\mathrm{Zr}} \cdot L_{\mathrm{Hf,Zr}}^L \\ & + {}^{ex}G_{\mathrm{B,Hf,Zr}}^L \end{aligned} \quad \text{(Eq 1)}$$

where R is the gas constant, and x_B, x_{Hf} and x_{Zr} are molar fractions of the elements B, Hf and Zr, respectively. The standard element reference (SER) state,[42] i.e. the stable structure of the element at 25 °C and 1 bar, is used as the reference state of Gibbs energy. The parameters $L_{i,j}^L\,(i,j = \mathrm{B,Hf,Zr})$ are the interaction parameters from the binary constituent systems. The ternary excess Gibbs energy ${}^{ex}G_{\mathrm{B,Hf,Zr}}^L$ is expressed as follows:

$$\begin{aligned} {}^{ex}G_{\mathrm{B,Hf,Zr}}^L = {} & x_{\mathrm{B}} \cdot x_{\mathrm{Hf}} \cdot x_{\mathrm{Zr}} \cdot \\ & \left(x_{\mathrm{B}} \cdot {}^{0}L_{\mathrm{B,Hf,Zr}}^L + x_{Hf} \cdot {}^{1}L_{\mathrm{B,Hf,Zr}}^L + x_{\mathrm{Zr}} \cdot {}^{2}L_{\mathrm{B,Hf,Zr}}^L \right) \end{aligned} \quad \text{(Eq 2)}$$

in which the interaction parameters ${}^{0}L_{\mathrm{B,Hf,Zr}}^L$, ${}^{1}L_{\mathrm{B,Hf,Zr}}^L$ and ${}^{2}L_{\mathrm{B,Hf,Zr}}^L$ are linearly temperature dependent. These parameters will be evaluated in the present work.

3.2 Solid Solution Phases

The Gibbs energies of the (βHf,βZr), (αHf,αZr) phases are described using two-sublattice models developed by Hillert and Staffansson[45] as $(\mathrm{Hf,Zr})_a(\mathrm{B,Va})_c$. In this model, it is assumed that Hf and Zr atoms occupy one sublattice while B atoms and vacancies occupy the other one, since B atoms are generally known to occupy only interstitial sites in these phases. The symbols a and c denote the numbers of sites on each sublattice and have values of $a = 1$ and $c = 3$ for the (βHf,βZr) phase; $a = 1$ and $c = 0.5$ for the (αHf,αZr) phase. For one formula unit $(\mathrm{Hf,Zr})_a(\mathrm{B,Va})_c$, the Gibbs energy of a phase is expressed as follows:

$$\begin{aligned} G_m^{\varphi} = {} & y'_{\mathrm{Hf}} \cdot y''_{\mathrm{B}} \cdot {}^{0}G_{\mathrm{Hf:B}}^{\varphi} + y'_{\mathrm{Zr}} \cdot y''_{\mathrm{B}} \cdot {}^{0}G_{\mathrm{Zr:B}}^{\varphi} \\ & + y'_{\mathrm{Hf}} \cdot y''_{\mathrm{Va}} \cdot {}^{0}G_{\mathrm{Hf:Va}}^{\varphi} + y'_{\mathrm{Zr}} \cdot y''_{\mathrm{Va}} \cdot {}^{0}G_{\mathrm{Zr:Va}}^{\varphi} \\ & + a \cdot RT \cdot (y'_{\mathrm{Hf}} \cdot \ln y'_{\mathrm{Hf}} + y'_{\mathrm{Zr}} \cdot \ln y'_{\mathrm{Zr}}) \\ & + c \cdot RT \cdot (y''_{\mathrm{B}} \cdot \ln y''_{\mathrm{B}} + y''_{\mathrm{Va}} \cdot \ln y''_{\mathrm{Va}}) \\ & + y'_{\mathrm{Hf}} \cdot y'_{\mathrm{Zr}} \cdot y''_{\mathrm{B}} \cdot L_{\mathrm{Hf,Zr:B}}^{\varphi} + y'_{\mathrm{Hf}} \cdot y'_{\mathrm{Zr}} \cdot y''_{Va} \cdot L_{\mathrm{Hf,Zr:Va}}^{\varphi} \\ & + y'_{\mathrm{Hf}} \cdot y''_{\mathrm{B}} \cdot y''_{\mathrm{Va}} \cdot L_{\mathrm{Hf:B,Va}}^{\varphi} \\ & + y'_{\mathrm{Zr}} \cdot y''_{\mathrm{B}} \cdot y''_{\mathrm{Va}} \cdot L_{\mathrm{Zr:B,Va}}^{\varphi} + y'_{\mathrm{Hf}} \cdot y'_{\mathrm{Zr}} \cdot y''_{\mathrm{B}} \cdot y''_{\mathrm{Va}} \cdot L_{\mathrm{Hf,Zr:B,Va}}^{\varphi} \end{aligned} \quad \text{(Eq 3)}$$

where y'_{Hf} and y'_{Zr} are the site fractions of Hf and Zr in the first sublattice, and y''_B and y''_{Va} are the site fractions of B and Va in the second sublattice. The parameter ${}^{0}G_{i:Va}^{\varphi}\,(i =$ Hf or Zr) is the Gibbs energy of pure element i, and the parameter ${}^{0}G_{i:B}^{\varphi}\,(i =$ Hf or Zr) is the Gibbs energy of a hypothetical state where all the interstitial sites are completely filled with B. $L_{\mathrm{Hf:B,Va}}^{\varphi}$, $L_{\mathrm{Hf,Zr:Va}}^{\varphi}$ and $L_{\mathrm{Zr:B,Va}}^{\varphi}$ are the binary parameters from the constituent binary systems, while the $L_{\mathrm{Hf,Zr:B}}^{\varphi}$ and $L_{\mathrm{Hf,Zr:B,Va}}^{\varphi}$ are the ternary parameters that will be optimized in the present assessment.

3.3 Compound Solution Phase HfB, ZrB_2, $(Hf,Zr)B_2$ and ZrB_{12}

The Gibbs energies of the HfB phase are described using the two-sublattice model $(\mathrm{Hf})_1(\mathrm{B,Hf})_1$ in present modeling. Considering that Zr preferentially replaces the atomic site of Hf in the B-Hf-Zr system,[39] the thermodynamic model for the HfB phase was developed to be $(\mathrm{Hf,Zr})_1(\mathrm{B,Hf})_1$, which is sufficient to cover the homogeneity range of HfB in the ternary system. Its molar Gibbs energy is given by the following expression:

$$
\begin{aligned}
G_m^{\mathrm{HfB}} = {} & y'_{\mathrm{Hf}} \cdot y''_{B} \cdot {}^{0}G_{\mathrm{Hf:B}}^{\mathrm{HfB}} + y'_{\mathrm{Hf}} \cdot y''_{\mathrm{Hf}} \cdot {}^{0}G_{\mathrm{Hf:Hf}}^{\mathrm{HfB}} + y'_{\mathrm{Zr}} \cdot y''_{\mathrm{B}} \cdot {}^{0}G_{\mathrm{Zr:B}}^{\mathrm{HfB}} + y'_{\mathrm{Zr}} \cdot y''_{\mathrm{Hf}} \cdot {}^{0}G_{\mathrm{Zr:Hf}}^{\mathrm{HfB}} \\
& + RT \cdot (y'_{\mathrm{Hf}} \cdot \ln y'_{\mathrm{Hf}} + y'_{\mathrm{Zr}} \cdot \ln y'_{\mathrm{Zr}}) + RT \cdot (y''_{\mathrm{B}} \cdot \ln y''_{\mathrm{B}} + y''_{\mathrm{Hf}} \cdot \ln y''_{\mathrm{Hf}}) \\
& + y'_{\mathrm{Hf}} \cdot y'_{\mathrm{Zr}} \cdot y''_{\mathrm{B}} \cdot L_{\mathrm{Hf,Zr:B}}^{\mathrm{HfB}} + y'_{\mathrm{Hf}} \cdot y'_{\mathrm{Zr}} \cdot y''_{\mathrm{Hf}} \cdot L_{\mathrm{Hf,Zr:Hf}}^{\mathrm{HfB}} + y'_{\mathrm{Hf}} \cdot y''_{\mathrm{B}} \cdot y''_{\mathrm{Hf}} \cdot L_{\mathrm{Hf:B,Hf}}^{\mathrm{HfB}} \\
& + y'_{\mathrm{Zr}} \cdot y''_{\mathrm{B}} \cdot y''_{\mathrm{Hf}} \cdot L_{\mathrm{Zr:B,Hf}}^{\mathrm{HfB}} + y'_{\mathrm{Hf}} \cdot y'_{\mathrm{Zr}} \cdot y''_{\mathrm{B}} \cdot y''_{\mathrm{Hf}} \cdot L_{\mathrm{Hf,Zr:B,Hf}}^{\mathrm{HfB}}
\end{aligned}
\qquad \text{(Eq 4)}
$$

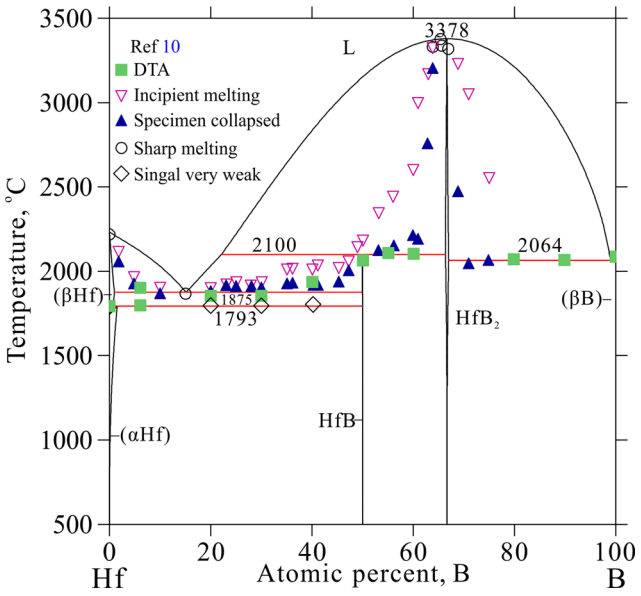

Fig. 2. Calculated B-Hf phase diagram with the HfB_2 and HfB phases modified in the present modeling, compared with the experimental data[10]

where ${}^{0}G_{\mathrm{Zr:B}}^{\mathrm{HfB}}$ and ${}^{0}G_{\mathrm{Zr:Hf}}^{\mathrm{HfB}}$ represent the Gibbs energy of the ideal equiatomic compounds ZrB and ZrHf.

The HfB_2 and $(Hf,Zr)B_2$ phases are modeled using two sublattices $(B,Hf)_1(B,Hf)_2$ and $(B,Hf,Zr)_1(B,Hf,Zr)_2$ in the binary B-Hf and ternary B-Hf-Zr systems, respectively. The ZrB_{12} phases are described with a two-sublattice model $(Hf,Zr)B_{12}$. Analogous expressions of formula (4) are employed to describe the Gibbs energy of these phases.

The ZrB phases was considered as a binary stoichiometric compound since no ternary experimental information was reported. According to the crystal structure of the (βB) phase (Pearson symbol: *hR*105) and the site occupations of the solute atoms in the unit cell,[46] the sublattice model $B_{93}(B,Zr)_{12}$ was adopted to describe the Gibbs energies of the (βB) phase in the B-Hf-Zr ternary system, which has been successfully used in the B-Zr[6] and B-C[46] systems.

Table 2 Calculated invariant reactions in the constituent binary B-Hf system.

Reaction	Type	Liquid composition (x_B) at.%	T, °C	Source
$L=HfB_2$	Congruent	66.7	3377	11
		66.66	3378	This work
$L+HfB_2=HfB$	Peritectic	22.0	2104	11
		22.13	2100	This work
$L=HfB_2+(\beta B)$	Eutectic	99.0	2065	11
		98.95	2064	This work
$L=(\beta Hf)+HfB$	Eutectic	15.0	1881	11
		15.15	1875	This work
$(\beta Hf)+HfB=(\alpha Hf)$	Peritectoid	…	1791	11
		…	1793	This work

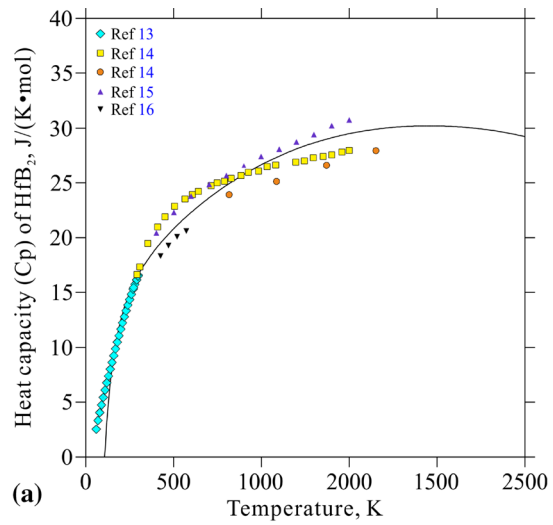
Ref 13
Ref 14
Ref 14
Ref 15
Ref 16
Heat capacity (Cp) of HfB_2, J/(K•mol)
Temperature, K
(a)

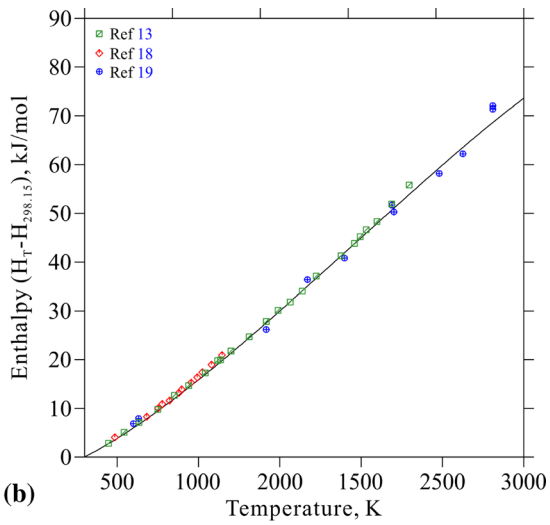
Ref 13
Ref 18
Ref 19
Enthalpy (H_T-$H_{298.15}$), kJ/mol
Temperature, K
(b)

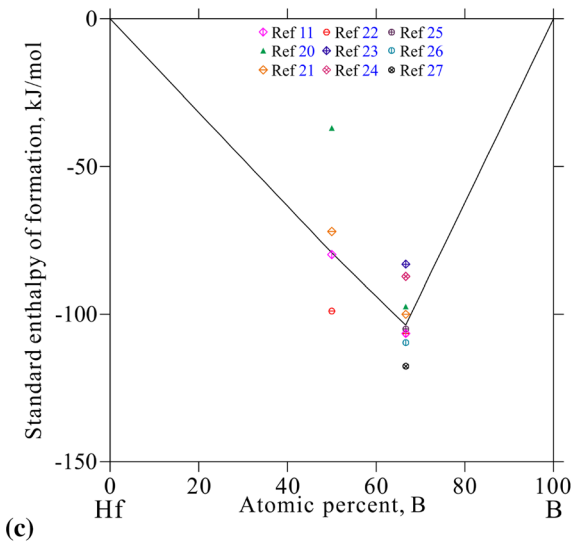
Ref 11
Ref 22
Ref 25
Ref 20
Ref 23
Ref 26
Ref 21
Ref 24
Ref 27
Standard enthalpy of formation, kJ/mol
Hf
Atomic percent, B
B
(c)

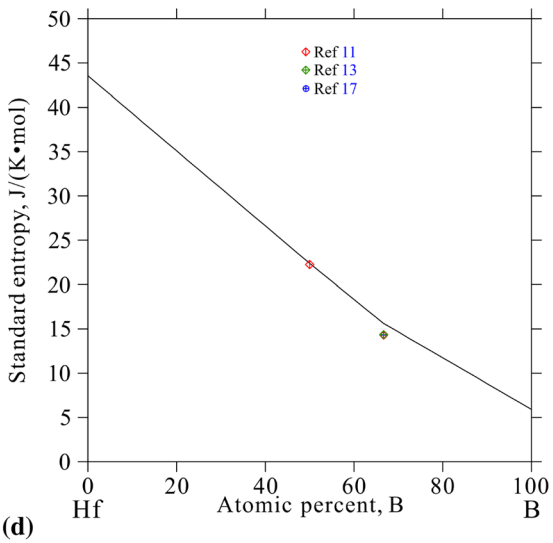
Ref 11
Ref 13
Ref 17
Standard entropy, J/(K•mol)
Hf
Atomic percent, B
B
(d)

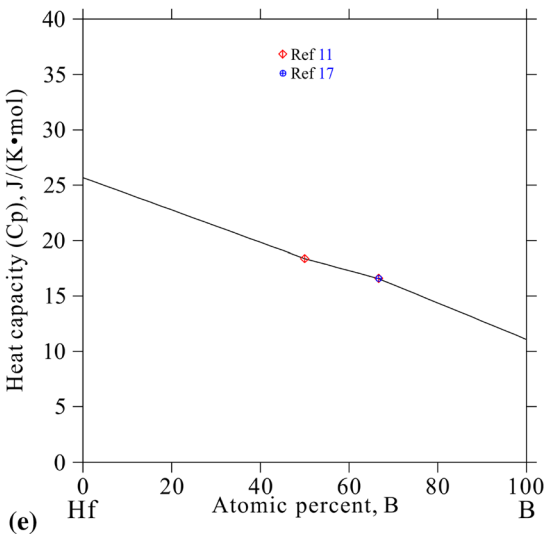
Ref 11
Ref 17
Heat capacity (Cp), J/(K•mol)
Hf
Atomic percent, B
B
(e)

◀**Fig. 3.** Calculated heat capacity of HfB_2 (a), enthalpy (H-$H_{298.15}$) (b), standard enthalpy of formation with the reference states of hcp Hf and (βB) at 298.15 K (c), standard entropy (d) and heat capacity (e), together with the experimental data[11,13,17,20-27]

All phases in this system and the corresponding thermodynamic models used in the present work are listed in Table 1.

4 Results and Discussion

The evaluation of the model parameters was carried out using the optimization program PARROT,[47] which works by minimizing the sum of the squares of the differences between measured and calculated values. The step-by-step optimization procedure described by Du et al.[48] was utilized in the present assessment. Each piece of selected information was given a certain weight based on the uncertainties of the experimental data. The weights were changed by trial and error during the assessment until most of the selected experimental information was reproduced within the expected uncertainty limits.

4.1 The B-Hf System

The assessment of the HfB_2 and HfB phases was based on the reported melting temperature, homogeneity range, heat capacity, entropy, and enthalpy of formation.[11,13,14,18-27] Fig. 2 presents the modified phase diagram of the B-Hf system, in comparison with the experimental results from Rudy and Windisch.[10] It can be seen that all the phase equilibria information related to the HfB_2 and HfB can be well reproduced by the present modeling. The calculated liquidus of L/(L+HfB_2) was much higher than the specimen collapse temperatures determined by Rudy and Windisch,[10] which was accepted as reasonable in the work from Bittermann and Rogl[11] and present modeling. Comparison of the calculated invariant reactions in the system with the previous modeling results[11] is listed in Table 2.

Figure 3a shows the calculated heat capacity of the HfB_2 phase together with the experimental data from Ref 13-16.

Table 3 Summary of the optimized thermodynamic parameters in the B-Hf-Zr system

Liquid: Model $(B,Hf,Zr)_1$

$${}^0L^{\text{Liquid}}_{\text{B,Hf,Zr}} = 302331.23 + 182.32T \quad {}^1L^{\text{Liquid}}_{\text{B,Hf,Zr}} = 563484.38 - 232.75T \quad {}^2L^{\text{Liquid}}_{\text{B,Hf,Zr}} = 717825.10 - 284.24T$$

(βHf,βZr): Model $(Hf,Zr)_1(B,Va)_3$

$${}^0L^{(\beta\text{Hf},\beta\text{Zr})}_{\text{Hf,Zr:B}} = 2072159.59$$

$(Hf,Zr)B_2$: Model $(B,Hf,Zr)_1(B,Hf,Zr)_1$

$${}^0G^{(\text{Hf,Zr})\text{B2}}_{\text{B:Hf}} = {}^0G^{\text{B}}_{(\beta\text{B})} + 2{}^0G^{\text{Hf}}_{\text{hcp}} + 36154.56 \qquad {}^0G^{(\text{Hf,Zr})\text{B2}}_{\text{Hf:Hf}} = 3{}^0G^{\text{Hf}}_{\text{hcp}} + 190739.12$$

$${}^0G^{(\text{Hf,Zr})\text{B2}}_{\text{Hf:B}} = 2{}^0G^{\text{B}}_{(\beta\text{B})} + {}^0G^{\text{Hf}}_{\text{hcp}} - 305018.73 - 82.27T + 13.66T\ln(T) - 0.010401397T^2 + 1.49775\text{E}-06T^3 - 450137.172T^{-1}$$

$${}^0G^{(\text{Hf,Zr})\text{B2}}_{\text{Hf:Zr}} = {}^0G^{\text{Hf}}_{\text{hcp}} + 2{}^0G^{\text{Zr}}_{\text{hcp}} + 100000 \qquad {}^0G^{(\text{Hf,Zr})\text{B2}}_{\text{Zr:Hf}} = 2{}^0G^{\text{Hf}}_{\text{hcp}} + {}^0G^{\text{Zr}}_{\text{hcp}} + 100000$$

$${}^0L^{(\text{Hf,Zr})\text{B2}}_{\text{Hf,Zr:B}} = -3508.56 + 7.84T \qquad {}^2L^{(\text{Hf,Zr})\text{B2}}_{\text{Hf,Zr:B}} = -5.50T$$

(Hf,Zr)B: Model $(Hf,Zr)_1(B,Hf)_1$

$${}^0G^{(\text{Hf,Zr})\text{B}}_{\text{Hf:B}} = {}^0G^{\text{B}}_{(\beta\text{B})} + {}^0G^{\text{Hf}}_{\text{hcp}} - 158537.05 + 4.69T \qquad {}^0G^{(\text{Hf,Zr})\text{B}}_{\text{Hf:Hi}} = 2{}^0G^{\text{Hf}}_{\text{hcp}} + 129867.07$$

$${}^0G^{(\text{Hf,Zr})\text{B}}_{\text{Zr:B}} = {}^0G^{\text{B}}_{(\beta\text{B})} + {}^0G^{\text{Zr}}_{\text{hcp}} - 78141.24 \qquad {}^0G^{(\text{Hf,Zr})\text{B}}_{\text{Zr:Hf}} = {}^0G^{\text{Hf}}_{\text{hcp}} + {}^0G^{\text{Zr}}_{\text{hcp}}$$

$${}^0L^{(\text{Hf,Zr})\text{B}}_{\text{Hf,Zr:B}} = -114031.681 \qquad {}^1L^{(\text{Hf,Zr})\text{B}}_{\text{Hf,Zr:B}} = 21.95T$$

All parameters are given in J/mole and temperature (T) in K. The Gibbs energies for the pure elements are taken from the compilation of Dinsdale.[42] The thermodynamic parameters in the B–Zr, Hf-Zr and B-Hf binary sub-systems are taken from Pan et al.,[6] Bittermann and Rogl[38] and Bittermann and Rogl[11] with the HfB_2 and HfB phases modified in the present work, respectively.

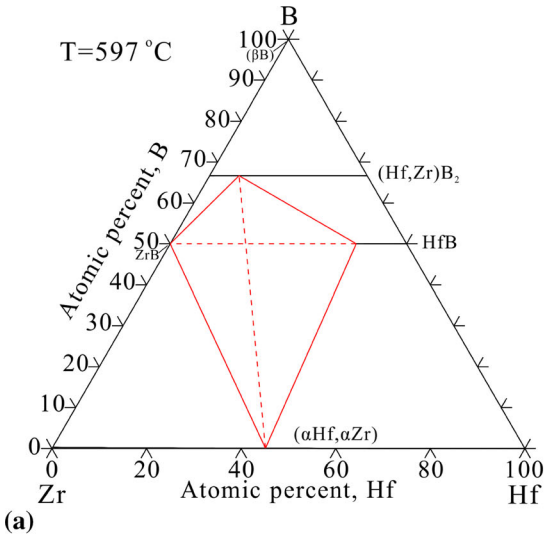
T=597 °C
B
100
(βB)
90
80
70
60
50
ZrB
40
30
20
10
0
Atomic percent, B
(Hf,Zr)B2
HfB
(αHf,αZr)
0
20
40
60
80
100
Zr
Atomic percent, Hf
Hf
(a)

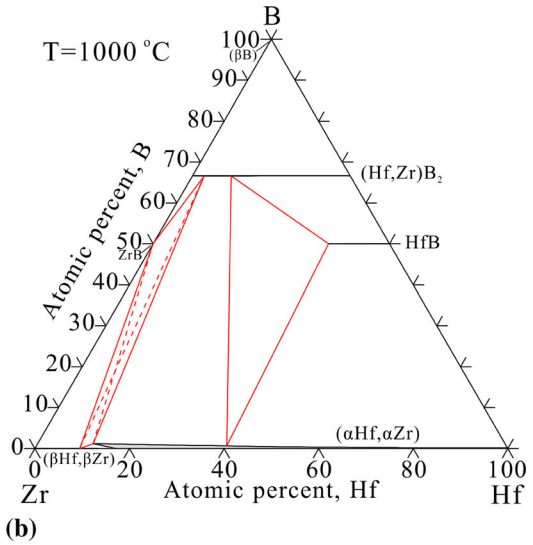
T=1000 °C
B
100
(βB)
90
80
70
60
50
ZrB
40
30
20
10
0
Atomic percent, B
(Hf,Zr)B2
HfB
(βHf,βZr)
(αHf,αZr)
0
20
40
60
80
100
Zr
Atomic percent, Hf
Hf
(b)

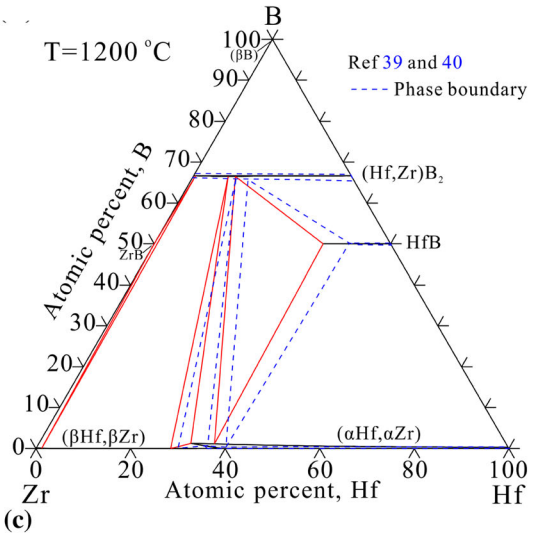
T=1200 °C
B
100
(βB)
90
80
70
60
50
ZrB
40
30
20
10
0
Atomic percent, B
Ref 39 and 40
Phase boundary
(Hf,Zr)B2
HfB
(βHf,βZr)
(αHf,αZr)
0
20
40
60
80
100
Zr
Atomic percent, Hf
Hf
(c)

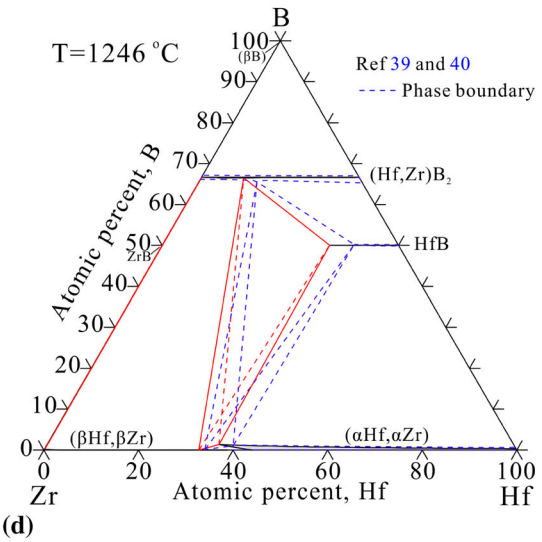
T=1246 °C
B
100
(βB)
90
80
70
60
50
ZrB
40
30
20
10
0
Atomic percent, B
Ref 39 and 40
Phase boundary
(Hf,Zr)B2
HfB
(βHf,βZr)
(αHf,αZr)
0
20
40
60
80
100
Zr
Atomic percent, Hf
Hf
(d)

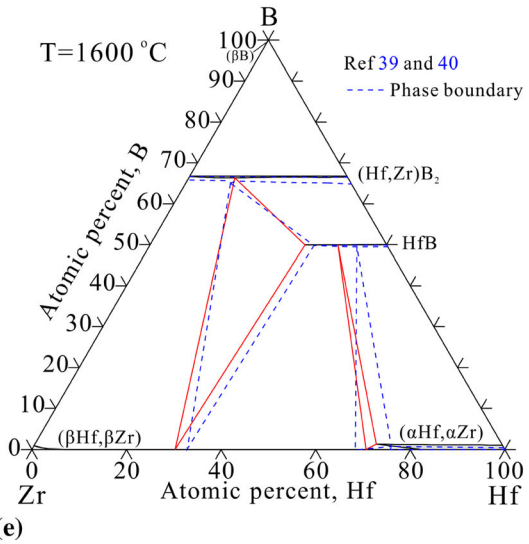
T=1600 °C
B
100
(βB)
90
80
70
60
50
40
30
20
10
0
Atomic percent, B
Ref 39 and 40
Phase boundary
(Hf,Zr)B2
HfB
(βHf,βZr)
(αHf,αZr)
0
20
40
60
80
100
Zr
Atomic percent, Hf
Hf
(e)

◀**Fig. 4** Calculated isothermal sections of the B-Hf-Zr system at 597 °C (a), 1000 °C (b), 1200 °C (c), 1246 °C (d) and 1600 °C (e), compared with the experimental data reported by Ref 39 and 40

The calculated results are well compatible with experimental ones. It should be underlined that the experiment data are quite dispersive at high temperatures. Large uncertainty may be induced by the defects, such as vacancies, dislocations, grain boundaries, and non-stoichiometry, and the errors introduced by the instruments. Thus, more elaborate experiments and theoretical predictions are still needed for clear depiction of thermodynamic properties of HfB_2. As show in Fig 3b the temperature dependencies of the enthalpy of HfB_2 referred to room temperatures ($H\text{-}H_{298.15}$), i.e., enthalpy of heating, obtained by calorimetric technique[13,18,19] are reproduced remarkably well by the present thermodynamic description. The standard enthalpies of formation referred to hcp Hf and (βB), standard entropies and heat capacities (Cp) of B-Hf alloys (solid lines) are presented in Fig. 3c, d and e, respectively. The results of the present thermodynamic descriptions agree properly with the experimental results.[11,13,17,20-27]

4.2 The B-Hf-Zr System

Based on the isothermal sections below 1700 °C,[39,40] the modeling of the B-Hf-Zr system proceeded with the solid phase. Therefore, the thermodynamic parameters of HfB, $(Hf,Zr)B_2$, and (βHf,βZr) phases were firstly evaluated. Subsequently, the interaction parameters for the liquid phase were then adjusted to reproduce the experimental data of isothermal sections above 1700 °C, vertical sections as well as the invariant equilibria.[39,40] Finally, the thermodynamic parameters for all the phases were optimized simultaneously by taking into account all of the selected phase diagram information.

Table 3 presents the thermodynamic parameters of the B-Hf-Zr system obtained from the present modeling. Based on these thermodynamic parameters, all phase equilibrium data are calculated to demonstrate the reasonability of the present assessment including isothermal sections, vertical sections and liquidus projection.

Figure 4a-e presents the calculated isothermal sections in comparison with the measured ones from Ref 39 and 40 at 597, 1000, 1200, 1246 and 1600 °C, respectively. The calculated phase relationships fit well with the experimental ones. In addition, three solid invariant reactions: $(Hf,Zr)B_2$+(αHf,αZr)=HfB+ZrB at 597 °C, $(Hf,Zr)B_2$+(-βHf,βZr)=(αHf,αZr)+ZrB at 1000 °C and (βHf,βZr)+HfB=$(Hf,Zr)B_2$ +(αHf,αZr) at 1246 °C can be found from the calculated results. The solubility of Zr in HfB was calculated to be 10.67 at.% at 597 °C and the solubility of Hf in ZrB was set to be zero in the whole temperature range. When the temperature exceeded 1600 °C, the binary phase ZrB disappeared. In the temperature range from 597 to 3230 °C, the hafnium and the zirconium diborides form continuous solid solution $(Hf,Zr)B_2$.

Figure 5a-e shows the calculated sections at 1675, 1700, 2020, 2500 and 3300 °C. The liquid phase forms in the Zr-rich corner and its domain gradually increases with increasing temperature. The discrepancies for the phase boundary of the liquid in Fig. 5c-d are mainly caused by different binary phase diagrams adopted by the literature [39,40] and present modeling. When the temperatures reaches 3300 °C, the liquid phase dominates the ternary system, ZrB_2 phase melts congruently and the $(Hf,Zr)B_2$ shrinks towards the B-Zr side.

The calculated vertical sections $Zr_{70}B_{30}$-$Hf_{70}B_{30}$ and $Zr_{50}B_{50}$-$Hf_{50}B_{50}$ of the B-Hf-Zr system are shown in Fig. 6a-b. Satisfactory agreement can be found between the calculated results and experimentally determined phase equilibria. Figure 6c illustrates the calculated $Hf_{33.33}B_{66.67}$-$Zr_{33.33}B_{66.67}$ vertical section, revealing the isomorphous reaction of L/$(Hf,Zr)B_2$. The experimentally determined melting signals are lower than the calculated ones, which may be caused by the compositions of the samples prepared by Harmon[39] and Rudy[40] not being in the single $(Hf,Zr)B_2$ phase region, resulting in the impurity phases (βB) or (Hf,Zr) in the alloys. Figures 7-8 show the temperatures and compositions of the three quasi-binary univariant reactions:

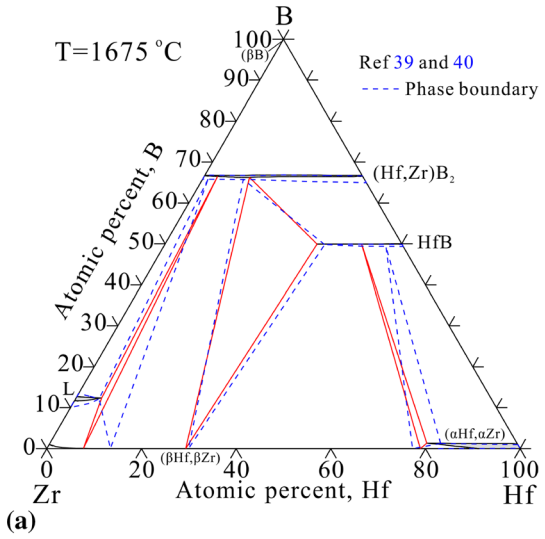
T=1675 °C
Ref 39 and 40
Phase boundary
B
(βB)
(Hf,Zr)B2
HfB
(αHf,αZr)
(βHf,βZr)
L
Atomic percent, B
Atomic percent, Hf
Zr
Hf

(a)

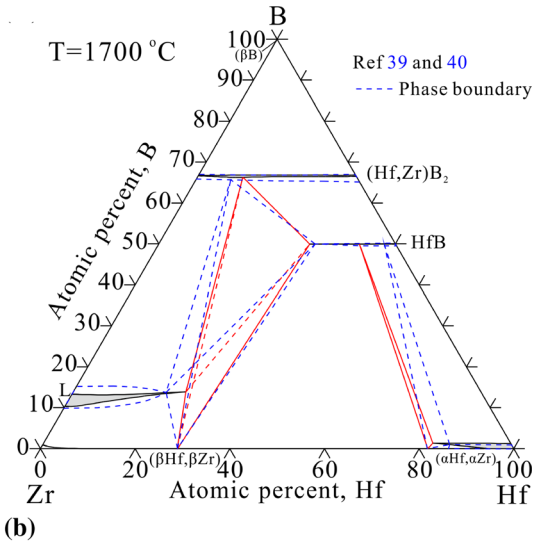
T=1700 °C
Ref 39 and 40
Phase boundary
B
(βB)
(Hf,Zr)B2
HfB
(αHf,αZr)
(βHf,βZr)
L
Atomic percent, B
Atomic percent, Hf
Zr
Hf

(b)

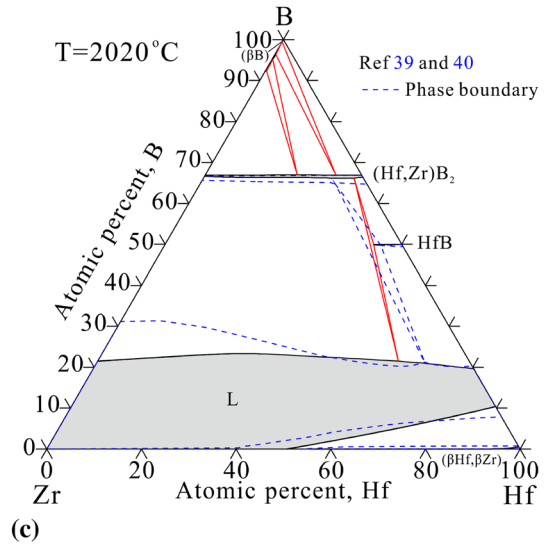
T=2020 °C
Ref 39 and 40
Phase boundary
B
(βB)
(Hf,Zr)B2
HfB
(βHf,βZr)
L
Atomic percent, B
Atomic percent, Hf
Zr
Hf

(c)

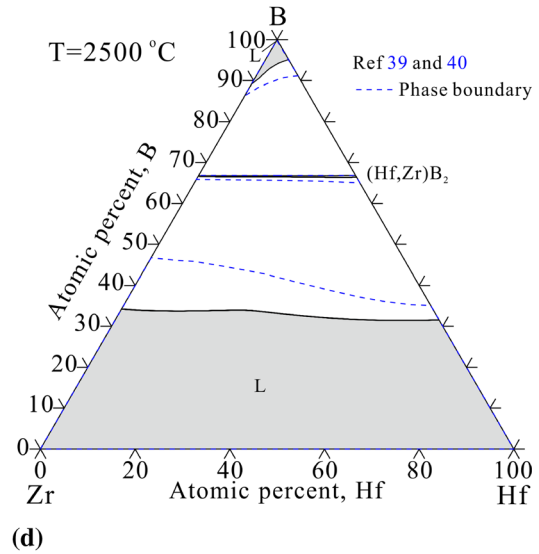
T=2500 °C
Ref 39 and 40
Phase boundary
B
(Hf,Zr)B2
L
Atomic percent, B
Atomic percent, Hf
Zr
Hf

(d)

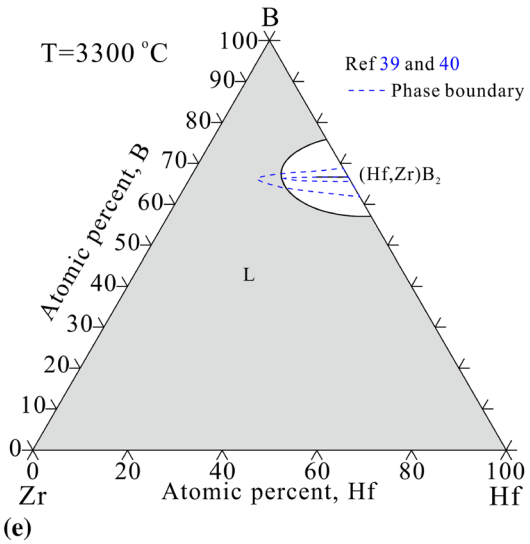
T=3300 °C
Ref 39 and 40
Phase boundary
B
(Hf,Zr)B2
L
Atomic percent, B
Atomic percent, Hf
Zr
Hf

(e)

◀**Fig. 5** Calculated isothermal sections of the B-Hf-Zr system at 1675 °C (a), 1700 °C (b), 2020 °C (c), 2500 °C (d) and 3300 °C (e), compared with the experimental data reported by Ref 39 and 40

L=(Hf,Zr)$_2$B+(βHf,βZr) and L=HfB+(βHf,βZr) in the B-Hf-Zr ternary system, together with the experimental results by Harmon[39] and Rudy.[40] Most of the experimental data are satisfactorily accounted for by the

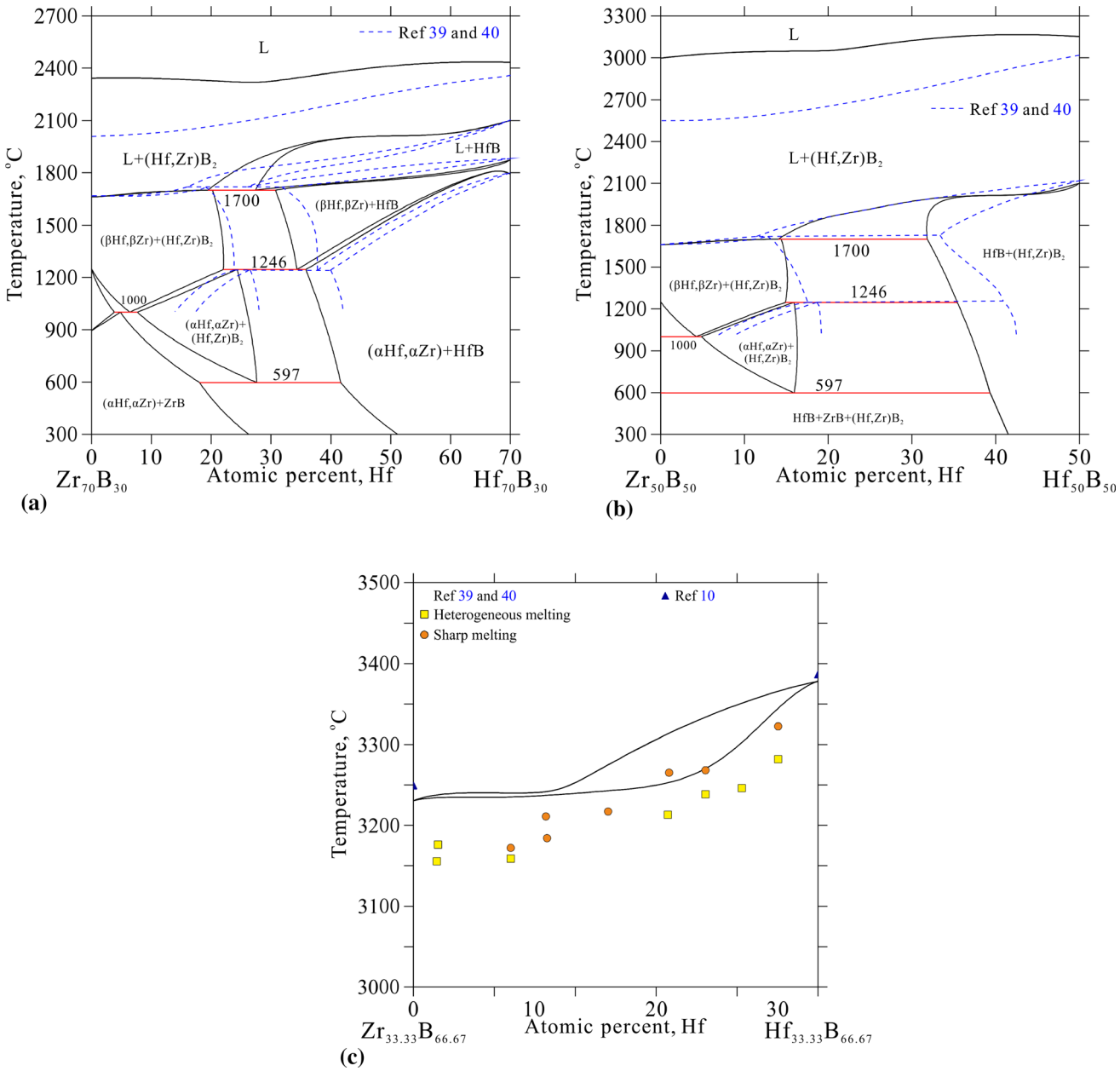

Fig. 6. Calculated vertical sections of the B-Hf-Zr system: (a) $Hf_{70}B_{30}$-$Zr_{70}B_{30}$, (b) $Hf_{50}B_{50}$-$Zr_{50}B_{50}$ and (c) $Hf_{33.33}B_{66.67}$-$Zr_{33.33}B_{66.67}$, together with the experimental data reported by Ref 39 and 40

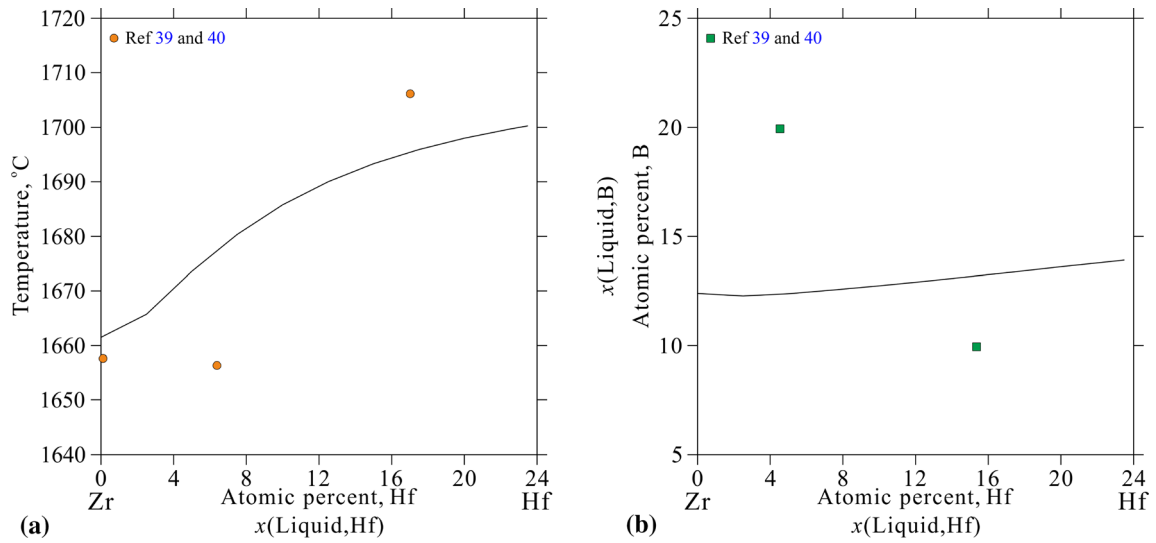

Fig. 7. Calculated temperatures (a) and compositions (b) of the quasi-binary univariate reaction of L=(Hf,Zr)$_2$B+(βHf,βZr), in comparison with the experimental results by Ref 39 and 40

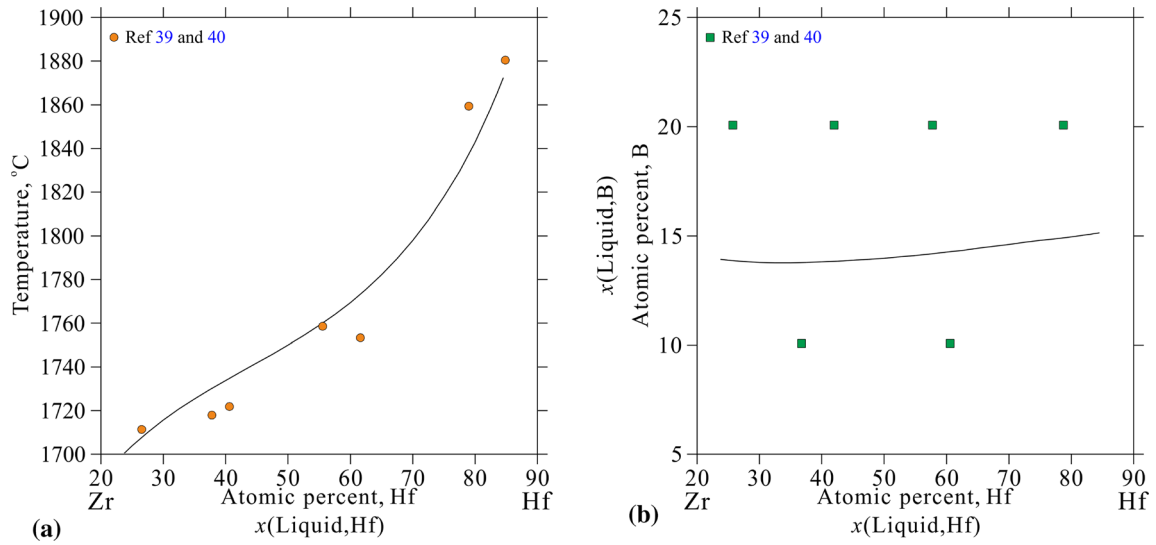

Fig. 8. Calculated temperatures (a) and compositions (b) of the quasi-binary univariate reaction of L=HfB+(βHf,βZr), in comparison with the experimental results by Ref 39 and 40

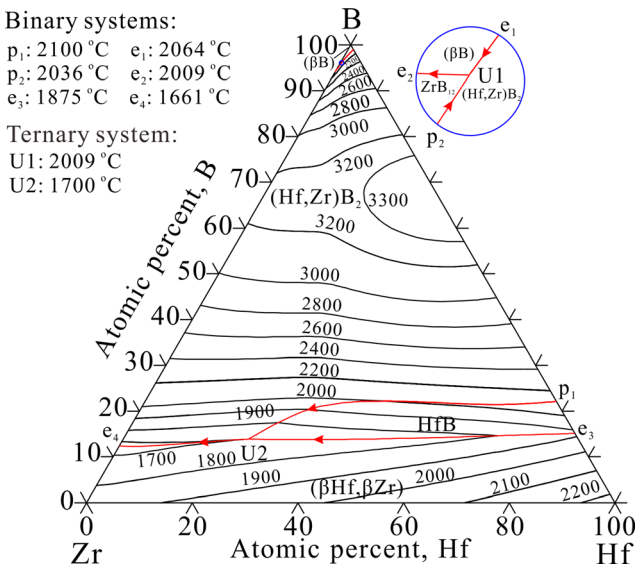

Fig. 9. Calculated liquidus projection of the B-Hf-Zr system according to the present thermodynamic modeling

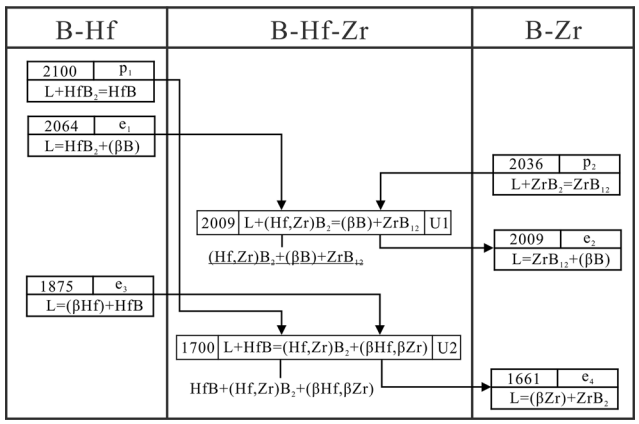

Fig. 10. Reaction scheme for the B-Hf-Zr system with participation of liquid phase according to the present calculations with temperature in °C

present calculation. The calculated liquidus projection of the B-Hf-Zr system is given in Fig. 9, while Figure 10 presents the reaction scheme in the range of melting/solidification for this system. The calculated invariant equilibria along with the experimental ones[39,40] are listed in Table 4. The reaction types, temperatures and compositions of the invariant reactions reported by Ref [39] and [40] are well reproduced by the present modeling.

5 Conclusions

Based on sufficient experimental information, the thermodynamic re-modelling of the constituent binary B-Hf and the novel description of the ternary B-Hf-Zr systems have been conducted by the CALPHAD method. A set of reasonable parameters for each phase in this system are obtained which can well reproduce the selected phase equilibria and thermodynamic properties of the constituent binary B-Hf system and the phase equilibrium relationships of the ternary system over the whole composition and temperature ranges including vertical sections, isothermal sections, and invariant reactions. The liquidus projection and reaction scheme of B-Hf-Zr system are also calculated according to the present optimization, which is very important for practical applications and basic material research. The complete database is attached, aiming to serve as a guide to experiment design, to allow further improvements and integration into higher order thermodynamic databases as well as to be used in microstructure simulation software.

Table 4 Comparison between the calculated and measured[39,40] invariant reactions with participation of liquid phase in the B-Hf-Zr system.

Invariant reaction	Composition of liquid phase, at.%			T, °C	Source
	B	Hf	Zr		
U1: L+(Hf,Zr)B_2= (βB)+ZrB_{12}	95.72	0.20	4.08	2009	This work
	…	…	…	2020	39, 40
U2: L+HfB= (Hf,Zr)B_2+(βHf, βZr)	13.93	23.79	62.28	1700	This work
	13.35	20.05	66.60	1715	39, 40

Acknowledgments The financial support from the National Natural Science Foundation of China (51901063), the Fundamental Research Funds for the Central Universities of China (JZ2021HGTB0094 and PA2021GDGP0059) is greatly acknowledged.

References

1. S. Bajpai, R. Kundu, and K. Balani, Effect of B4C Reinforcement on Microstructure, Residual Stress, Toughening and Scratch Resistance of (Hf,Zr)B2 Ceramics, *Mater. Sci. Eng. A*, 2020, **796**(7), p 140022.
2. F. Monteverde, F. Saraga, and M. Gaboardi, Compositional Disorder and Sintering of Entropy Stabilized (Hf,Nb,Ta,Ti,Zr)B2 Solid Solution Powders, *J. Eur. Ceram. Soc.*, 2020, **40**(12), p 3807–3814.
3. J. Yin, B.H. Zhang, X.J. Liu, and Z.R. Huang, Pressurelessly Densified $(Zr,Hf)_B2$-SiC Ceramics by Co-Doping Hafnium-Boron Carbides, *J. Alloys Compd.*, 2017, **727**(15), p 706–710.
4. L. Silvestroni, and D. Sciti, Effects of $MoSi_2$ Additions on the Properties of Hf– and Zr–B2 Composites Produced by Pressureless Sintering, *Scripta Mater.*, 2007, **57**, p 165–168.
5. M. Brochu, B. Gauntt, T. Zimmerly, A. Ayala, and R. Loehman, Fabrication of UHTCs by Conversion of Dynamically Consolidated Zr+B and Hf+B Powder Mixtures, *J. Am. Ceram. Soc.*, 2008, **91**(9), p 2815–2822.
6. Y.F. Pan, C. Zhang, J.X. Zhang, L. Huang, X.Y. Yang, Y. Du, and F.H. Luo, Thermodynamic Modeling of the B-Ti-Zr System over the Whole Composition and Temperature Ranges, *J. Phase Equilib. Diffus.*, 2019, **40**, p 364–374.
7. J.O. Andersson, T. Helander, L. Hoglund, P. Shi, and B. Sundman, Thermo-Calc & DICTRA Computational Tools for Materials Science, *Calphad*, 2002, **26**(2), p 273–312.
8. L. Zhang, I. Steinbach, and Y. Du, Phase-Field Simulation of Diffusion Couples in the Ni–Al System, *Int. J. Mater. Res.*, 2011, **102**(4), p 371–380.
9. P. Rogl, and P.E. Potter, A Critical Review and Thermodynamic Calculation of the Binary System: Hafnium-Boron, *Calphad*, 1988, **12**(3), p 207–218.
10. E. Rudy and S. Windisch, Ternary Phase Equilibriums in Transition Metal-Boron-Carbon-Silicon Systems. Technical Report No. AFML-TR-65-2, Part I, Volume IX, 1965
11. H. Bittermann, and P. Rogl, Critical Assessment and Thermodynamic Calculation of the Ternary System Boron-Hafnium-Titanium (B-Hf-Ti), *J. Phase Equilib.*, 1997, **18**(1), p 24–47.
12. V.T. Witusiewicz, A.A. Bondar, U. Hecht, O.A. Potazhevska, and T. Ya Velikanova, Thermodynamic Modelling of the Ternary B-Mo-Ti System with Refined B-Mo Description, *J. Alloys Compd.*, 2016, **655**, p 336–352.
13. A.S. Bolgar, and A.V. Blinder, Thermodynamic Characteristics of Hafnium and Tantalum Diboride in A Wide Temperature Range, *Sov. Powder Metall. Metal Ceram.*, 1989, **28**, p 128–131.
14. H.L. Schick, *Thermodynamics of Certain Refractory Compounds*. Academic Press, New York, 1966.
15. I. Barin, *Thermochemical Data of Pure Substances*, 3rd edn. Wiley-VCH Verlag Gmbh, Weinheim, 1995.
16. R. Loehman, E. Corral, H.P. Dumm, P. Kotula, and R. Tandon, Ultra High Temperature Ceramics for Hypersonic Vehicle Applications, SAND2006-2925, Albuquerque, 2006
17. E.F. Westrum, and G. Feick, Heat Capacities of $HfB_{2.035}$ and $HfC_{0.968}$ from 5 to 350 K, *J. Chem. Thermodyn.*, 1977, **9**(3), p 293–299.
18. R. Mezaki, E.W. Tilleux, D.W. Barnes, and J.L. Margrave, High-Temperature Thermodynamic Properties of Some Refractory Borides, *Thermodyn. Nucl. Mater.*, IAEA Publications Proceeding Series, Vienna, 1962, pp 775–788
19. C.D. Pears, S. Oglesby, and D.S. Nell, The Thermal Properties of Twenty-Six Solid Materials to 5000 °C or Their Destruction Temperatures, Tech. Report ASD-TDR-62-765, Wright-Patterson A.F.B.,OH, 1963
20. Y. Pan, H.W. Huang, X. Wang, and Y.H. Lin, phase Stability and Mechanical Properties of Hafnium Borides: A First-Principles Study, *Comput. Mater. Sci.*, 2015, **109**, p 1–6.
21. C.W. Xie, Q. Zhang, H.A. Zakaryan, H. Wan, N. Liu, A.G. Kvashnin, and A.R. Oganov, Stable and Hard Hafnium Borides: A First-Principles Study, *J. Appl. Phys.*, 2019, **125**(20), p 205109.
22. L.A. Mcclaine, Thermodynamic and Kinetic Studies for a Refractory Material Program, Tech. Report No. ASD-TDR-62-204, Part III, Wright-Patterson A.F.B., OH, 1964
23. E.P. Kitpichev, Y.I. Rubtsov, T.V. Sorokina, and V.K. Prokudina, Standard Enthalpies of Formation of Some Group IV-V Element Borides, *J. Phys. Chem.*, 1979, **53**(8), p 1128–1130.
24. V.M. Maslov, A.S. Neganov, I.P. Borovinskaya, and A.G. Merzhanov, Self-Propagating High-Temperature Synthesis as a Method of Determining Heats of Formation of Refractory Compounds, *Fiz. Goreniya Vzryva*, 1978, **14**(6), p 73–82.
25. P.J. Spencer, O. Kubaschewski-von Goldbeck, R. Ferro, R. Marazza, K. Girgis, and O. Kubaschewski, Hafnium, Physico-Chemical Properties of its Compounds and Alloys, K.L. Komarek, Ed., Atomic Energy Review, Special Issue 8, IAEA, Vienna, 1981
26. G.K. Johnson, E. Greenberg, J.L. Margrave, and W.N. Hubbard, Fluorine Bomb calorimetry, Enthalpies of Formation of the diborides of zirconium and hafnium, *J. Chem. Eng. Data*, 1967, **12**(1), p 137–141.
27. H.L. Schick, Thermodynamics of Certain Refractory Compounds, Academic Press, New York, 1966, **1**, p 240-247
28. F.W. Glaser, and B. Post, *Trans. AIME*, 1953, **197**, p 1117–1118.
29. E. Rudy and S. Windisch, Ternary Phase Equilibriums in Transition Metal-Boron-Carbon-Silicon Systems. Technical Report No. AFML-TR-65-2, Part I, Volume VIII, 1966
30. K.P. Portnoi, V.M. Romashov, and L.I. Vyroshina, Constitution Diagram of the System Zirconium-Boron, *Poroshkov. Metall.*, 1970, **91**, p 68–71.
31. K.I. Portnoi, and V.M. Romashov, Binary Constitution Diagrams of Systems Composed of Various Elements and Boron - A Review, *Poroshkov. Metall.*, 1972, **5**, p 48–56.
32. H. Nowotny, E. Rudy, and F. Benesovsky, Investigations in the Systems: Zirconium-Boron-Carbon and Zirconium-Boron-Nitrogen, *Monatsh Chem.*, 1960, **91**, p 963–974.
33. O.I. Shulishova, and I.A. Shcherbak, Superconductivity of the Borides of Transitions and Rare-Earth Metals, *Inorg. Mater.*, 1967, **3**(8), p 1304–1306.
34. J.S. Haggerty, J.L. O'Brien, and J.F. Wenckus, Growth and Characterization of Single Crystal ZrB_2, *J. Cryst. Growth*, 1968, **3**(4), p 291–294.
35. Y. Champion, and S. Hagege, A Study of Composite Interfaces in the Zr-ZrB_2 System, *J. Mater. Sci. Lett.*, 1992, **11**, p 290–293.
36. Y. Champion, and S. Hagege, Experimental Determination and Symmetry Related Analysis of Orientation Relationships in Heterophase Interfaces: a Case Study in the Zr-B System, *Acta Mater.*, 1996, **44**(10), p 4169–4179.
37. Y. Champion, and S. Hagege, Structural Analysis of Phases and Heterophase Interfaces in the Zirconium-Boron System, *J. Mater. Sci.*, 1998, **33**, p 4035–4041.
38. H. Bittermann, and P. Rogl, Critical Assessment and Thermodynamic Calculation of the Ternary System C-Hf-Zr (Carbon-Zirconium-Hafnium), *J. Phase Equilib.*, 2002, **23**(3), p 218–235.

39. D.P. Harmon, Ternary Phase Equilibria in Transition Metal-Boron-Carbon-Silicon Systems Technical Report No. AFML-TR-65-2, Part II, Volume XI, 1965
40. E. Rudy, Ternary Phase Equilibria in Transition Metal-Boron-Carbon-Silicon Systems. Technical Report No. AFML-TR-65-2, Part V, 1969
41. G. Cacciamani, P. Riani, and F. Valenza, Equilibrium Between MB_2 (M = Ti, Zr, Hf) UHTC and Ni: A Thermodynamic Database for the B-Hf-Ni-Ti-Zr System, *Calphad*, 2011, **35**, p 601–619.
42. A.T. Dinsdale, SGTE Data for Pure Elements, *Calphad*, 1991, **15**(4), p 317–425.
43. O. Redlich, and A.T. Kister, Thermodynamics of Nonelectrolytic Solutions. Algebraic Representation of Thermodynamic Properties and the Classification of Solutions, *Ind. Eng. Chem.*, 1948, **40**, p 84–88.
44. Y.M. Muggianu, M. Gambino, and J.P. Bros, Enthalpies of Formation of Liquid Alloys Bismuth-Gallium-Tin at 723.Deg.K Choice of an Analytical Representation of Integral and Partial Excess Functions of Mixing, *J. Chim. Phys. Phys. Chim. Biol.*, 1975, **72**(1), p 83–88.
45. M. Hillert, and L.-I. Staffansson, The Relationship Between Gibbs Free Energy and the Intersection of the Liquidi in Phase Diagrams of Reciprocal Systems, *Metall. Trans. B*, 1975, **6B**, p 613–616.
46. P. Rogl, J. Vřešt'ál, T. Tanaka, and S. Takenouchi, The B-rich Side of the B-C Phase Diagram, *Calphad*, 2014, **44**, p 3–9.
47. B. Sundman, B. Jansson, and J.O. Andersson, The Thermo-Calc Databank System, *Calphad*, 1985, **9**, p 153–190.
48. Y. Du, R. Schmid-Fetzer, and H. Ohtani, Thermodynamic Assessment of the V-N System, *Z. Metallkd.*, 1997, **88**, p 545–556.